ZAMM- JOURNAL OF APPLIED MATHEMATICS AND MECHANICS

https://onlinelibrary.wiley.com/journal/15214001

Impact factor:1.603

Accepted June 15th 2022

"Numerical study of natural convection dissipative electro-magnetic non-Newtonian flow through a non-Darcy channel"

Lijun Zhang[1], M. M. Bhatti[1*], O. Anwar Bég[2], Henry J. Leonard[2] and S. Kuharat[2]

[1]College of Mathematics and Systems Science, Shandong University of Science and Technology, Qingdao 266590, Shandong, **China**.

[2]Multi-Physical Engineering Sciences Group, Mechanical Engineering, Salford University, School of Science, Engineering and Environment (SEE), Manchester, M54WT, **UK**.

*Correspondence: mmbhatti@sdust.edu.cn

ABSTRACT: Inspired by simulating duct thermal processing of novel functional polymers, a novel mathematical model is developed for buoyancy-driven heat transfer in non-Newtonian Williamson fluid flow in a vertical parallel plate duct containing a permeable medium, under mutually orthogonal electrical and magnetic fields. The momentum equation features electrical and magnetic body force terms and the Darcy-Brinkman-Forchheimer mode is used for non-Darcy effects. The energy balance equation includes thermal buoyancy (natural convection body force) and a modified viscous dissipation term. The conservation equations with associated boundary conditions are re-framed into a system of coupled non-linear ordinary differential equations via appropriate similarity transformations. The emerging dimensionless boundary value problem is then solved with a differential transform method (DTM). Validation of DTM solutions with the bvp4c MATLAB collocation solver is included. The influence of key parameters on velocity, temperature and average Nusselt number, are computed and illustrated graphically. With elevation in Weissenberg (non-Newtonian) number, velocity and temperature are reduced. Velocity is suppressed with increasing non-Darcian parameter (Forchheimer effect) whereas it is enhanced with increment in buoyancy convection parameter. With increasing Forchheimer, Darcy number and Hartmann number, the average Nusselt number is boosted whereas it is decreased with higher values of buoyancy convection parameter, Brinkman number, and Weissenberg number. A strong reduction in temperature is computed with increment in ratio of Joule electrical heating to heat conduction parameter. DTM is shown to be an exceptionally accurate and versatile approach for simulating non-Newtonian electromagnetohydrodynamic transport in ducts.

KEYWORDS: *Natural convection; Williamson fluid; permeable medium; Differential transform method; non-Darcy model.*

1. INTRODUCTION

Natural convection [1] is driven by thermal buoyancy forces and features in multiple technological and environmental systems including heat exchangers, granular and fiber insulation, petroleum reservoirs, enclosure fire dynamics, geothermal systems, nuclear waste repositories, packed beds, porous insulation, energy efficient drying, food processing, grain storage, and chemical catalytic reactors. Many emerging applications simultaneously feature natural convection in *both Newtonian and non-Newtonian flows*, for example, in thermal duct processing and chemical engineering [2, 3]. Non-Newtonian fluids exhibit complex material (stress-strain) characteristics which cannot be simulated with a conventional Newtonian model. Important phenomena include shear-thinning (pseudoplastic) behaviour, stress relaxation, retardation etc [4]. Porous media may also be deployed to control heat and flow characteristics in natural convection systems. Shenoy [5] has described many models of non-Newtonian buoyancy-driven convection flows in porous media in areas including biomechanics, chemical engineering, geophysics, industrial engineering, petroleum engineering, ceramic engineering, food technology, groundwater hydrology, mechanical engineering and soil mechanics. *Newtonian natural convection* studies include Haghighi *et al*. [6] investigated natural convection using a new plate-fin design with heat sinks. Dutta *et al.* [7] explored the entropy generation by natural convection in a quadrilateral enclosure with non-isothermal heating at the lower wall. Ma *et al.* [8] used a Lattice Boltzmann method and water-based nanofluids to examine the positional impact of a heated obstacle on natural convection and heat transmission in a U-shaped enclosure. Nia *et al.* [9] investigated natural convection in an L-shaped enclosure with baffles using the Lattice Boltzmann method. Jha and Samaila [10] derived similarity solutions for natural convection flow over a vertical plate under the influence of thermal radiation. Dash and Dash [11] used a computational approach to investigate natural convection in a vertical thick hollow cylinder, under the influence of non-uniform heating, Dutta *et al.* [12] investigated the entropy generation and heat transmission mechanism with natural connection through a rhombic enclosure. Non-Newtonian natural convection studies have utilized many different rheological constitutive equations to simulate a variety of industrial liquids. Lee [13] deployed the Ostwald-deWaele power-law model and asymptotic methods to investigate thermal buoyancy effects in transport in non-Newtonian polymers in a vertical channel. Srinivas and Bég [14] utilized the Eringen micropolar model, homotopy analysis and second law thermodynamic approaches to compute the entropy generation in fully developed flow and heat transfer in a vertical channel under thermal buoyancy effects. Singh *et al.* [15] applied the short memory Walters-B viscoelastic fluid model to study combined free and forced convective in reactive electrically conducting vertical channel transport. Further studies have implemented the Saffman dusty fluid-particle model [16], Bingham viscoplastic model [17], a third grade viscoelastic Reiner-Rivlin fluid [18] and more recently the Johnson-Segalman elastic-viscous model [19]. All these studies identified a significant modification in heat and momentum transfer characteristics with non-Newtonian effects and substantial deviation from Newtonian results.

In real-world applications, *viscous dissipation* often arises. This involves local thermal energy generation through kinetic energy dissipation and frequently occurs in non-Newtonian transport and also viscous flows through porous materials. Viscous heating can

therefore exert a significant modification to temperature and velocity distributions. Unlike other thermal influences on fluid motion (such as buoyancy forces caused by cooled or heated walls, and localized heat sources/sinks), the impact of heat produced owing to viscous dissipation can be prominent both in forced convection and natural or mixed convection flows. Gebhart [20] conducted a pioneering study of viscous heating in the presence of thermal buoyancy effects, noting that it contributes significantly when the induced kinetic energy is of similar magnitude to the amount of heat transferred. He deployed perturbation methods to show that viscous heating also strongly modifies thermal characteristics under both isothermal and uniform-flux wall surface conditions. Martin [21] used an integral profile procedure is used to compute viscous heating effects on laminar flow development in a uniform pipe under adiabatic conditions and strong thermal buoyancy. Further studies of viscous dissipative convection with buoyancy effects include El-Din [22] (who deployed a Brinkman number to characterize dissipation), Umavathi and Bég [23] (who also considered dual species diffusion in addition to natural convection and mixed wall boundary conditions), Mishra *et al.* [24] (who examined squeezing natural convection in a magnetic sensor channel with non-Fourier heat flux) and Ajibade and Umar [25] (who used a homotopy perturbation method to study wall thickness heat conduction and heat source/sink effects). These studies generally showed that temperatures are strongly elevated whereas Nusselt numbers are reduced with viscous heating effects. In the context of non-Newtonian fluids, polymeric flows have been confirmed to produce much greater viscous heating effects than Newtonian fluids. It has been emphasized in several studies including Cox and Macosko [26] and Winter [27] that substantial viscous heating is produced even at very low Reynolds numbers in die flows, molten polymer shear flows and thermal duct systems. More recently Hassan *et al.* [28] have further identified that viscous heating in polymer injection mould filling in vertical channels acts as an energy source. They used a Cross viscoelastic model and a finite volume numerical technique to study the dissipative buoyancy-driven transport of liquid polystyrene (PS) and polypropylene (PP) polymers in a vertical channel. Several investigators have also considered alternative rheological models to examine non-Newtonian dissipative convection in channel flows. Akbar *et al.* [29] employed the Casson viscoplastic model and MATLAB software to study metachronal propulsion in a vertical channel of magnetized polymeric fluids including wall hydrodynamic slip and thermal jump effects. Ragueb and Mansouri [30] applied a power-law (pseudoplastic/dilatant) model and Alternating Direction Implicit an to investigate dissipative natural convection flow in a vertical isothermal elliptic cross-section duct. Again, all these studies confirmed the marked modifications in thermal distributions computed when viscous dissipation is present.

In many industrial duct systems [31], as noted earlier, *porous media* are also utilized. They provide an inexpensive mechanism for controlling velocity and heat transfer in natural convection flows. They can be synthesized from foams, fibrous materials, packed spheres and other materials. Both isotropic (constant permeability) and anisotropic (variable permeability) systems are deployed. For low Reynolds number (viscous dominated) scenarios, to simulate the pressure drop across the porous medium, the classical model used is the Darcy model, as elaborated by Shenoy [5]. This provides a reasonable approximation when inertial effects are neglected. However, at higher velocities, inertial drag cannot be ignored. The inertial effects are particularly prominent when the medium has high porosity

or when the flow rate is large; the linear Darcy model breaks down and does not achieve good accuracy. Higher flow velocities characterize certain industrial transport processes in porous medium ducts, including filtration, thermal management and slurry dynamics. The divergence from linearity utilized in the momentum equation for porosity effects must be accounted for in such problems. The Forchheimer terms, which represent quadratic drag is significant for larger particle Reynolds numbers as noted by Nakayama *et al.* [32]. Owing to greater filtration velocities, quadratic drag develops in the momentum equation for porous media, and the drag form due to solid obstacles becomes comparable to surface drag due to friction [33]. Since Reynolds number is related to the particle diameter, Bear and Braester [13] have emphasized that the flow becomes *non-Darcian* when the Reynolds number exceeds very low values (typically about 10). Physically, flow deviates inside the medium, whereas theoretically, the velocity and pressure gradient have a non-linear relationship. Non-Darcy models are therefore also required for non-Newtonian flows [34-36]. Muskat [37] investigated porous inertial effects using the Forchheimer component in the momentum equation. Brinkman [38] proposed a viscous diffusion model to consider boundary frictional drag which also characterizes vorticity diffusion near the wall. Collectively when both approaches are combined the resulting model is known as the Darcy-Brinkman-Forchheimer nonlinear porous medium model. When Brinkman friction is neglected, the relevant model is the Darcy-Forchheimer nonlinear model. When Forchheimer inertial (second order) drag is neglected the Darcy-Brinkman model is deployed. All four models i.e. *Darcian, Darcy-Forcheimmer, Darcy-Brinkman and Darcy-Brinkman-Forchheimer models* have proven extremely popular in recent years. Non-Newtonian Darcy flow in transient natural convection of viscoelastic fluids has been examined by Zhao *et al.* [39]. Tripathi and Bég [40] utilized the Darcy-Brinkman model to quantify the periodic peristaltic propulsion of Maxwell viscoelastic fluids through a porous medium. The Darcy-Forcheimmer model was implemented by Alomar *et al.* [41] to simulate the natural convection in a two-dimensional porous enclosure It has also been deployed by Bég *et al.* [42] in unsteady rotating channel flows and by Bég *et al.* [43] for two-phase natural convection in biofluid transport in non-Darcian porous media. However, these models of non-Darcy flow neglected the influence of Forccheimer effect on viscous heating. More recently it has been shown that the Forchheimer quadratic drag term contributes to the dissipation, despite the fact, that, the viscosity does not enter explicitly. This idea has been implemented by Al-Hadhrami *et al.* [44] for variable permeability scenarios. Their non-Darcy dissipative formulation reduces to that for a fluid clear of solid material in the case where the Darcy number (dimensionless permeability parameter) tends to infinity. Umavathi *et al.* [45] has elaborated on how the Brinkman term be treated in the same way as the Darcy and Forchheimer terms, so that the total viscous dissipation remains equal to the power of the total drag force. The *modified non-Darcy model* is therefore required to properly characterize viscous dissipation effects in porous media transport.

In recent years, a new generation of *intelligent fluent media* have emerged which respond to electrical and /or magnetic fields and also possess rheological properties. Examples include electroconductive polymers (ECPs) [46], functional gels [47] and ferro-rheological fluids [48]. Such smart fluids with multi-functionality also have potential application for electrical devices, actuators, sensors and biomedical devices [49]. These

developments have motivated interest in mathematical modelling of electrohydrodynamic (EHD), magnetohydrodynamic (MHD) and also combined electromagnetohydrodynamic (EMHD) flows of non-Newtonian media in duct and other systems, of relevance to materials processing and biomedical transport, both with and without porous media. To simulate the flows of such fluids, electromagnetohydrodynamic body forces must be considered in addition to non-Newtonian characteristics. The nonlinear nature of electro/magnetic rheological flows generally require numerical or powerful analytical methods to derive robust solutions. Manzoor *et al.* [50] deployed the Adomian decomposition solution to study magnetohydrodynamic (MHD) viscoelastic flow in a ciliated vertical channel containing a Darcian porous medium with viscous heating. Tripathi *et al.* [51] used perturbation methods to compute the electro-osmotic pumping of second order viscoelastic fluids in a biological channel under an axial electrical field. Bhatti *et al.* [52] investigated bio-inspired pumping of electromagnetic two-phase non-Newtonian (Jefferys) viscoelastic liquids in a porous medium channel with the Darcy model, under a transverse magnetic field and axial electrical field. Further investigations include Umavathi and Bég [53] who considered electromagnetic nanofluid dissipative flow with natural convection heat and mass transfer in a vertical duct [53], Tripathi *et al.* [54] (who examined polar couple stress pumping in electromagnetic flow in a vertical micro-channel, and Tripathi *et al.* [55] (who studied Debye electrical double layer effects in combined electro-magnetic transient wavy flow in a vertical channel). These studies have identified different effects are produced via magnetic and electrical body forces in thermal transport in duct flows and that judicious selection of electrical and magnetic field strengths are required to optimize performance.

In the present work, we consider the electro-magneto-hydrodynamic non-Newtonian natural convection through a vertical parallel plate duct containing an isotropic, homogenous non-Darcian porous medium. The Williamson model is deployed for the rheology. In the Williamson model [56-58], the apparent viscosity varies gradually between μ_0 at zero shear rate, and μ_∞ as the shear rate tends to infinity. This model provides an excellent approximation for certain electroconductive polymers [46]. The study is motivated by developing a more comprehensive model of functional electromagnetic rheological liquids which are increasingly being deployed in thermal processing. These provide enhanced features for improving working fluid performance and can be manipulated to adjust heat and momentum transfer rates. A Williamson model is deployed to represent the non-Newtonian characteristics. The *modified Darcy-Brinkman-Forchheimer model* in the energy equation additionally considers the effect of viscous dissipation. The solutions to the nonlinear coupled differential equations are obtained using a numerical technique known as the Differential transform Method (DTM) [59]. *The novelty of the present study is the simultaneous consideration of electrical and magnetic field effects, thermal buoyancy, a modified non-Darcy model and non-Newtonian characteristics*. The impact of key control parameters (e. g. Weissenberg number, buoyancy convection parameter, Forchheimer parameter etc) on momentum and heat transfer characteristics is evaluated in detail and visualized graphically. Tables are also included for validation of the DTM solutions with a MATLAB bvp4c solver. The present study to the authors' knowledge constitutes a novel contribution to the thermofluid dynamics of non-Newtonian functional materials processing. The simulations

will be useful to thermal process duct design using advanced intelligent electromagnetic rheological liquids.

2. MATHEMATICAL MODEL FOR ELECTROMAGNETIC NON-NEWTONIAN THERMAL TRANSPORT

The regime under consideration comprises steady-state buoyancy driven (natural convection) electromagnetic functional non-Newtonian Williamson polymer flow upwards in a vertical parallel plate channel, with the walls located at finite distance apart. The walls at $x = -b$ and $x = b$ hold a constant temperature $\tilde{T}_-$ and $\tilde{T}_+$, where $\tilde{T}_- > \tilde{T}_+$. A Cartesian coordinate system is considered (as shown in **Figure 1**).

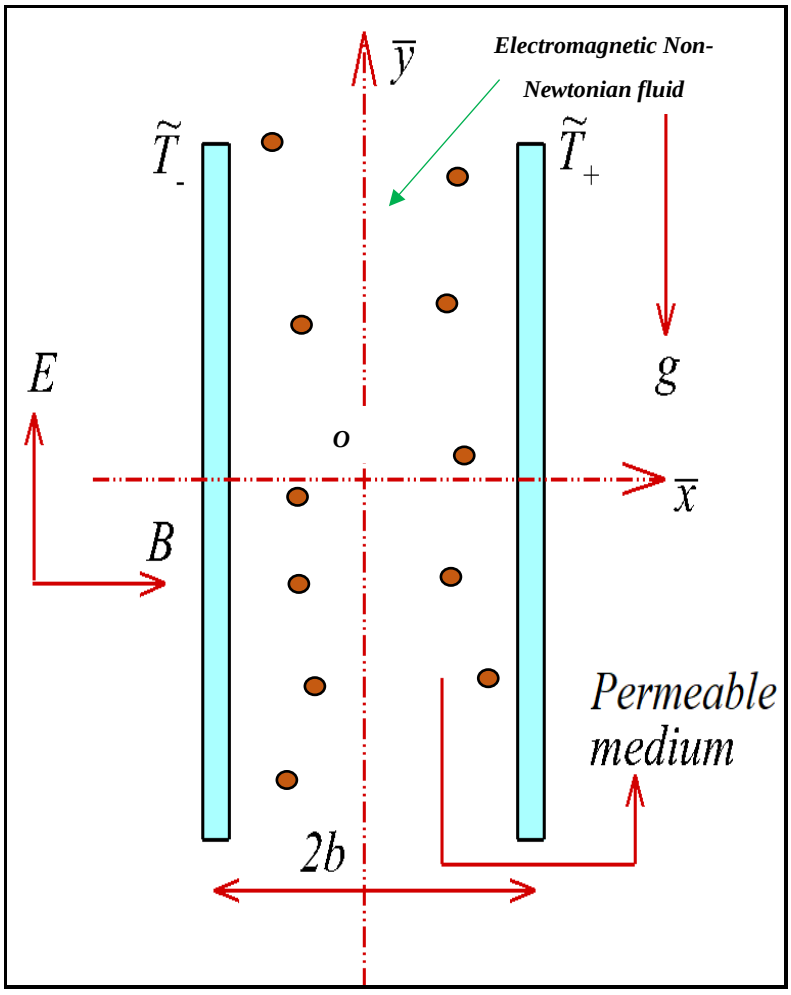

Figure 1: Geometrical model for natural convection Williamson fluid flow through a vertical duct containing a non-Darcy permeable medium.

The medium betwneen two vertical plates is considered to be an isotropic, non-deformable permeable medium and simulated via the *dissipation modified* Darcy-Brinkman-Forchheimer drag force model [44]. At the left wall, $x = -b$ and at the right wall, $x = b$. The electroconductive polymer is subjected to an axial electrical field and transverse magnetic field i.e. mututally orthogonal fields. Electro-magnetohydrodynamic (EMHD) flow is therefore mobilized in the channel. Hall current, ionslip and magnetic induction effects are

neglected since magnetic Reynolds numebr is too small for magnetic field distortion. The velocity field and the temperature field are considered as follows:

$$\mathbf{v} = v(\bar{x})\mathbf{j}, \quad \tilde{T} = \tilde{T}(\bar{x}), \tag{1}$$

In view of the proposed assumptions, the continuity, momentum, and the energy equations in vectorial form, are defined as [60-62]:

$$\nabla \cdot \vec{V} = 0, \tag{2}$$

$$\rho \frac{\mathrm{d}\mathbf{v}}{\mathrm{d}\tilde{t}} = \nabla \cdot \boldsymbol{\chi} - \nabla \cdot p + \vec{J} \times \vec{B} - \frac{\rho c_F}{\kappa^{1/2}} |\mathbf{v}| \mathbf{v} - \frac{\mu}{\kappa} \mathbf{v} + \rho g \beta \left(\tilde{T} - \tilde{T}_m \right), \tag{3}$$

$$\rho S_h \frac{d\tilde{T}}{d\tilde{t}} - \frac{\vec{J} \cdot \vec{J}}{\sigma} = \xi : \mathrm{grad}\, \mathbf{v} + \frac{\rho c_F}{\kappa^{1/2}} |\mathbf{v}| \mathbf{v}^2 + \frac{\mu}{\kappa} \mathbf{v}^2 - \nabla \cdot \vec{Q}, \tag{4}$$

Here g is gravity, p stands for the pressure, β is the thermal expansion coefficient, κ stands for the permeability (hydraulic conductivity of the porous medium), c_F denotes Forchheimer (quadratic porous drag) coefficient, ρ denotes density of the electroconductive polymer, $\tilde{t}$ stands for time, $\tilde{T}_m = \frac{1}{2}\left(\tilde{T}_- + \tilde{T}_+\right)$ represents mean reference temperature, $\vec{J}\left(=\sigma\left[\vec{V} \times \vec{B} + \vec{E}\right]\right)$ vector represents the local ion current density, σ represents the electrical conductivity, $\vec{B}$ is the static magnetic field, $\vec{E}$ is the electric field, $\frac{\mathrm{d}}{\mathrm{d}\tilde{t}}$ the material derivative, the symbol ":" indicate the double dot product, $\tilde{T}$ represents the temperature, S_h denotes the specific heat, and $\vec{Q}$ is the heat flux vector. The stress tensor $\boldsymbol{\chi}$ is for an incompressible non-Newtonian Williamson fluid, is defined as:

$$\boldsymbol{\chi} = \left[\mu_{\inf} + \frac{\mu - \mu_{\inf}}{1 - \dot{\gamma}\Lambda} \right] \vec{R}_1, \tag{5}$$

Here $\vec{R}_1$ represents the first Rivlin-Erickson tensor, μ represents the dynamic viscosity, $\mu_{\inf}$ represents the dynamic viscosity at infinity shear rate, Λ is the time constant, and $\dot{\gamma}$ i.e. shear rate is defined as

$$\dot{\gamma} = \sqrt{\frac{\Pi}{2}}, \Pi = \mathrm{trace}\left(\vec{R}_1^2\right), \tag{6}$$

where Π represents the second invariant tensor. By virtue of Eqns. (2-4), the pressure is assumed constant, and the reduced conservation equations for momentum and energy for the case $\mu_{\inf} = 0$, and $\dot{\gamma}\Lambda < 1$ now take the form:

$$\mu \frac{\mathrm{d}}{\mathrm{d}\bar{x}} \left[\frac{\mathrm{d}v}{\mathrm{d}\bar{x}} + \frac{\Lambda}{\sqrt{2}} \left(\frac{\mathrm{d}v}{\mathrm{d}\bar{x}} \right)^2 \right] - \sigma B^2 v + \sigma B E - \frac{\mu}{\kappa} v - \frac{c_F \rho}{\kappa^{1/2}} v^2 + \rho \beta g \left(\tilde{T} - \tilde{T}_m \right) = 0, \tag{7}$$

$$T_c\frac{\partial^2\tilde{T}}{\partial\bar{x}^2}+\mu\left(\frac{\mathrm{d}v}{\mathrm{d}\bar{x}}\right)\left[\frac{\mathrm{d}v}{\mathrm{d}\bar{x}}+\frac{\Lambda}{\sqrt{2}}\left(\frac{\mathrm{d}v}{\mathrm{d}\bar{x}}\right)^2\right]+\sigma\left(E^2+B^2v^2-2EBv\right)+\frac{\rho c_F}{\kappa^{1/2}}v^3+\frac{\mu}{\kappa}v^2=0. \quad (8)$$

Here T_c is the thermal conductivity of the electromagnetic polymer fluid. In Eqn. (8), the second term on the left-hand side indicates the *volumetric heat production due to viscous dissipation*, and the third composite electromagnetic term includes the *axial electrical body force, transverse magnetic body force* and the *Joule heating* term.

Their boundary conditions are defined at the left and right walls of the duct as follows:

$$\left.\begin{aligned}v(\bar{x})&=0,\\ \tilde{T}(\bar{x})&=\tilde{T}_+\end{aligned}\right] \quad \text{at} \quad \bar{x}=b,$$
$$\left.\begin{aligned}v(\bar{x})&=0,\\ \tilde{T}(\bar{x})&=\tilde{T}_-\end{aligned}\right] \quad \text{at} \quad \bar{x}=-b, \quad (9)$$

Eqns. (7,8) with boundary conditions (9) constitute a nonlinear, multi-degree boundary value problem. To facilitate a robust semi-numerical (DTM) solution and introduce scaling, it is judicious to define the following non-dimensional parameters:

$$v=\frac{v}{V_0},x=\frac{\bar{x}}{b},T=\frac{\tilde{T}-\tilde{T}_m}{\tilde{T}_--\tilde{T}_+}, \quad (10)$$

Here V_0 is a reference velocity. Implementing Eqn. (10) into Eqns. (7-9), yields the following dimensionless model:

$$\frac{\mathrm{d}^2v}{\mathrm{d}x^2}+We\frac{\mathrm{d}^2v}{\mathrm{d}x^2}\left(\frac{\mathrm{d}v}{\mathrm{d}x}\right)-M^2v+E_L-D_av-F_rv^2+G_rT=0, \quad (11)$$

$$\frac{\mathrm{d}^2T}{\mathrm{d}x^2}+B_r\left(\frac{\mathrm{d}v}{\mathrm{d}\bar{x}}\right)\left[\frac{\mathrm{d}v}{\mathrm{d}\bar{x}}+We\left(\frac{\mathrm{d}v}{\mathrm{d}\bar{x}}\right)^2\right]-E_mv+B_rM^2v^2+E+D_aB_rv^2+B_rF_rv^3=0, \quad (12)$$

The boundary conditions become:

$$T=\frac{1}{2},v(x)=0, \quad \text{at} \quad x=-1,$$
$$T=-\frac{1}{2},v(x)=0, \quad \text{at} \quad x=1, \quad (13)$$

It is important to note that the porous medium terms feature also in the energy balance eqn. (12) owing to the contribution of viscous dissipation in the modified non-Darcy formulation [44, 45]. Furthermore, T the dimensionless temperature, D_a represents the Darcy number (non-dimensional permeability of the porous medium), F represents the Forchheimer number (the non-Darcian second order drag parameter for porous media), M denotes a Hartmann number (ratio of Lorentz magnetic body force to viscous hydrodynamic force), E_L represents the dimensionless parameter related with the electrical field strength and is an *electrical Hartmann number* (ratio of electrical body force to viscous hydrodynamic force),

Gr_t is thermal Grashof number, G_r is the buoyancy convection parameter due to temperature gradient, Re is the Reynolds number, B_r represents the Brinkman number (expresses the ratio of heat produced due to viscous dissipation in heat transfer owing to molecular conduction); E_m specifies the ratio of Joule heating to heat conduction, E quantifies the influence of heat generation due to the interaction of electric and magnetic fields on heat conduction and *We* is the Weissenberg viscoelastic material parameter. These parameters are defined as follows:

$$D_a = \frac{b^2}{\kappa}, F_r = \frac{c_f V_0 b^2}{\upsilon\sqrt{\kappa}}, M^2 = \frac{\sigma}{\mu}B^2 b^2, E_L = \frac{\sigma b^2 EB}{V_0 \mu}, G_r = \frac{Gr_t}{Re_t \frac{\beta g b^3 (\tilde{T}_- - \tilde{T}_+)}{\upsilon^2}}$$

$$B_r = \frac{\mu V_0^2}{T_c(\tilde{T}_- - \tilde{T}_+)}, E_m = \frac{2\sigma EBV_0 b^2}{T_c(\tilde{T}_- - \tilde{T}_+)}, E = \frac{\sigma E^2 b^2}{T_c(\tilde{T}_- - \tilde{T}_+)}, We = \frac{\sqrt{2}V_0 \Lambda}{b}, Re = \frac{bV_0}{\upsilon}. \quad (14)$$

The Nusselt number, which measures the convective heat transfer relative to conduction heat transfer at the walls (channel plates), is written as follows:

$$Nu_{\text{ave}} = -\left(\frac{T'(1) + T'(-1)}{2}\right). \quad (15)$$

3. DIFFERENTIAL TRANSFORM METHOD (DTM) SOLUTIONS:

The dimensionless, coupled nonlinear boundary value problem defined by Eqns. (11) to (13) has been solved by the differential transform method (DTM). This is a powerful, rapidly convergent semi-analytical approach originally developed to solve nonlinear differential equations in electrical engineering circuit analysis. Later, DTM has been deployed to simulate many complex multi-physical nonlinear fluid dynamics problems including rotating biomagnetic flows [63], viscoelastic squeezing flows [64], non-Newtonian coating flows [65] and electromagnetic viscoplastic stretching sheet flows [66]. DTM is distinct from the more conventional higher-order Taylor series method by the fact that it involves extensive computations at higher orders. Iteratively, DTM achieves a polynomial series solution. It is a different procedure for locating analytic Taylor series solutions. A brief description of this approach is now given. Let us consider a function $y(t)$ which is analytic in domain *T* and consider $t = t_0$ represents any point in *T*. The function $y(t)$ is described by a power series for which t_0 is the allocated center point. The differential transform of the function $y(t)$ is given by:

$$Y(L) = \frac{1}{L!}\left[\frac{\mathrm{d}^L y(t)}{\mathrm{d}t^L}\right]_{t=t_0}, \quad (16)$$

Here $y(t)$ represents the original function and $Y(L)$ represents the transformed function. The inverse transformation is defined as:

$$y(t) = \sum_{L=0}^{\infty} t^L Y(L), \quad (17)$$

It follows that:

$$y(t)=\sum_{L=0}^{\infty}\frac{t^{L}}{L!}\left[\frac{\mathrm{d}^{L}y(t)}{\mathrm{d}t^{L}}\right]_{t=0}, \tag{18}$$

Eqn. (18) describes the concept of the differential transform which is obtained via the Taylor series method. However, in this technique, derivatives are *not evaluated symbolically*. Therefore, the function $y(t)$ can be expressed in terms of finite series as follows:

$$y(t)\cong\sum_{L=0}^{N}t^{L}Y(L), \tag{19}$$

This shows that $y(t)\cong\sum_{L=N+1}^{\infty}t^{L}Y(L)$ is small enough. The values of N help to determine the convergence rate of the series coefficient. In the next section, we will apply this technique to the formulated nonlinear differential equations. Further details of DTM are given in refs. [59,63-66].

4. SOLUTIONS USING DIFFERENTIAL TRANSFORM METHOD:

Nonlinear coupling exists between the transformed dimensionless differential equations (11-12) and their relevant boundary conditions (13). To find the solutions to these differential equations, we define the differential transformation for the formulated equations:

$$\begin{aligned}&(\varepsilon+1)(\varepsilon+2)H(\varepsilon+2)+We\sum_{s=0}^{\varepsilon}(\varepsilon+1-s)(k+2-s)(s+1)\xi(s+1)H(\varepsilon+2-r)\\&+E_{L}-M^{2}H(\varepsilon)-D_{a}H(\varepsilon)-F_{r}H(\varepsilon)^{2}+G_{r}\theta(\varepsilon)=0,\end{aligned} \tag{20}$$

$$\begin{aligned}&(\hbar+1)(\hbar+2)\theta(\hbar+2)+B_{r}\left[\begin{array}{l}\displaystyle\sum_{s=0}^{\varepsilon}(s+1)(\varepsilon+1-s)H(s+1)H(1-s+\varepsilon)+We\\\displaystyle\sum_{s_{1}=0}^{\varepsilon}\sum_{s=0}^{s_{1}}H(s+1)H(s_{1}-s+1)H(1-s_{1}+\varepsilon)\\\times(s+1)(s_{1}-s+1)(1-s_{1}+\varepsilon)\end{array}\right]\\&-E_{m}H(\varepsilon)+B_{r}M^{2}H(\varepsilon)^{2}+E+B_{r}D_{a}H(\varepsilon)^{2}+B_{r}F_{r}H(\varepsilon)^{3}=0,\end{aligned} \tag{21}$$

where $H(\varepsilon)\&\theta(\varepsilon)$ are the differential transforms of the functions $v(x)\&T(x)$. The function transformation is a key stage in DTM. The boundary conditions for the current simulation are specified as follows:

$$\begin{aligned}&U(-1)=0,\qquad\theta(-1)=\frac{1}{2},\\&U'(-1)=\eta_{\alpha},\quad\theta'(-1)=\eta_{\beta},\end{aligned} \tag{22}$$

Following the differential transform procedure, the boundary conditions in the preceding equations become:

$$\begin{aligned}&H(-1)=0,\qquad\theta(-1)=\frac{1}{2},\\&H'(-1)=\eta_{\alpha},\quad\theta'(-1)=\eta_{\beta}.\end{aligned} \tag{23}$$

Introducing Eqn. (23) in Eqns. (20-21) and invoking a recursive scheme, we can obtain other values of $H(\varepsilon)$ and $\theta(\varepsilon)$. With the help of boundary conditions $H(1)=0, \theta(1)=0$, one may determine η_α & η_β. The following are the possible final solutions:

$$v \cong \sum_{\varepsilon=0}^{i} H(\varepsilon) x^k, \quad T \cong \sum_{\varepsilon=0}^{i} \theta(\varepsilon) x^k. \tag{24}$$

All the computations have been performed in Mathematica software.

5. VALIDATION WITH MATLAB BVP4C

To validate the DTM solutions, an alternative numerical procedure known as bvp4c has also been deployed. This method employs collocation formula in the Matlab bvp4c software [67-68]. An appropriate convergence criterion is used, and excellent correlation is achieved with the DTM solutions for the average Nusselt number, for a variety of emerging parameter values, as documented in **Table 1**. Confidence in the present DTM solutions is therefore justifiably very high.

Table 1: Comparison of DTM and Matlab bvp4c results for average Nusselt number with selected parameters for $D_a = 0.1,\ F_r = 0.3,\ B_r = 7, We = 0.2, M = 0.5, G_r = 0.1, E_L = 1, E_m = 1, E = 1$ unless otherwise indicated.

D_a	F_r	M	Gr	B_r	We	E_m	E	Nu_{ave} (DTM)	Nu_{ave} (MATLAB bcp4c)
0								0.14486079	0.14487001
1								0.31576534	0.31578210
	0							0.13704600	0.13704600
	0.5							0.18861026	0.18864212
		0						0.10225558	0.102257053
		0.4						0.14748864	0.147496393
			0.1					0.26912537	0.269135487
			0.15					0.22430119	0.224300312
				6				0.23242452	0.232431001
				6.5				0.20212672	0.202130519
					0			0.43489232	0.434910436
					0.5			-0.13198822	-0.13197981
						0.6		0.17283961	0.17284102
						0.7		0.17561053	0.17560994
							0.6	0.19520738	0.19520624
							0.7	0.18905662	0.18905814

Table 1. also shows that increment in Darcy number (*Da*), Forchheimer number (*Fr*), and all three electromagnetic parameters (*M, E_m and E*) all increase the average Nusselt number profile, whereas the Grashof number (*Gr*), the Weissenberg viscoelastic number (*We*), and the Brinkman number (*Br*) i. e. dissipation parameter, all reduce magnitudes of the average Nusselt number profile. Clearly therefore *heat transfer rate to the duct wall* is elevated with stronger electromagnetic and greater permeability and non-Darcy effects whereas it is suppressed with stronger thermal buoyancy, viscoelasticity and viscous heating effects (since these parameters increase temperatures in the core flow in the duct).

6. GRAPHICAL AND NUMERICAL ANALYSIS

The graphical and numerical results of velocity, temperature, and average Nusselt number profile for selected parameters are presented in this section. The parametric values have been selected based on [30] as follows: $D_a = 0.1,\ F_r = 0.3,\ B_r = 7,$ $We = 0.2, M = 0.5, G_r = 0.1, E_L = 1, E_m = 1, E = 1.$ These correspond to realistic practical values for electromagnetic polymers with weak thermal buoyancy effects, in highly permeable porous media, with strong viscous dissipation and intermediate electrical and magnetic field strengths [46, 47].

Figures 2-4 visualize the average Nusselt number distributions on the duct wall with selected parameters.

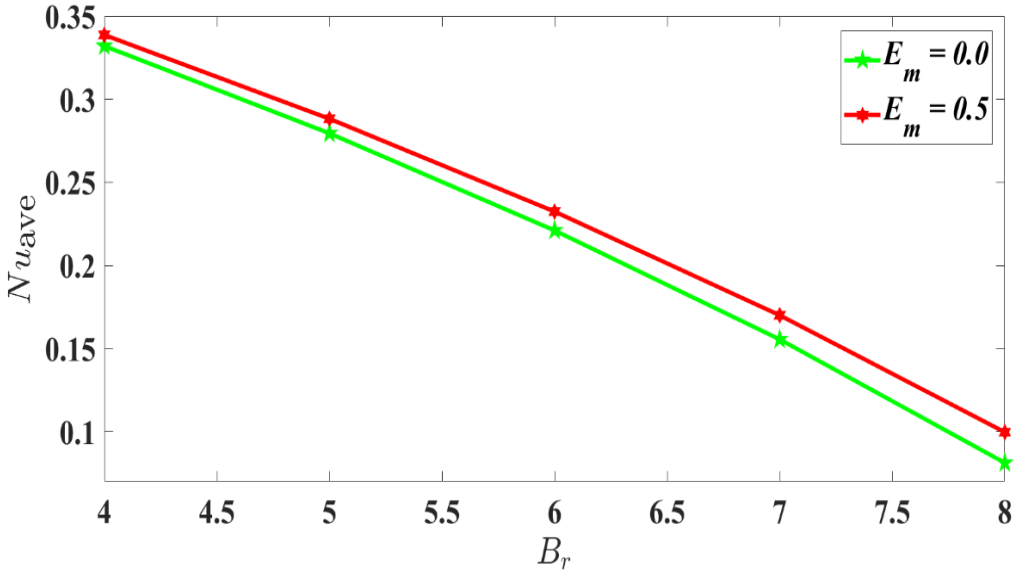

Figure 2. Average Nusselt number profile *versus* Brinkman number against multiple values of E_m.

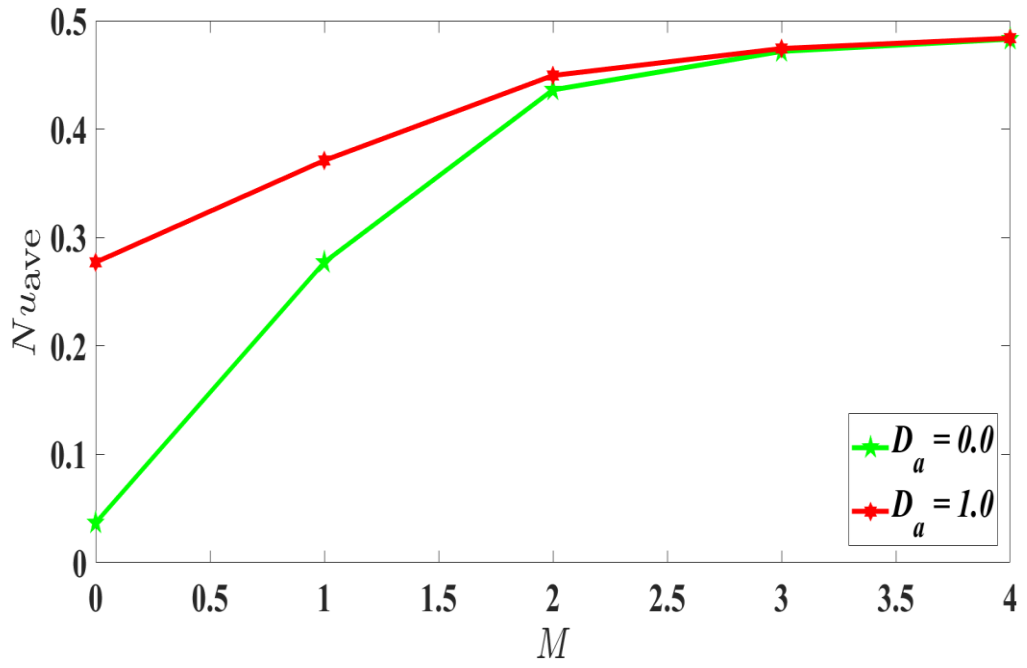

Figure 3. Average Nusselt number profile *versus* Hartmann magnetic number against multiple values of D_a.

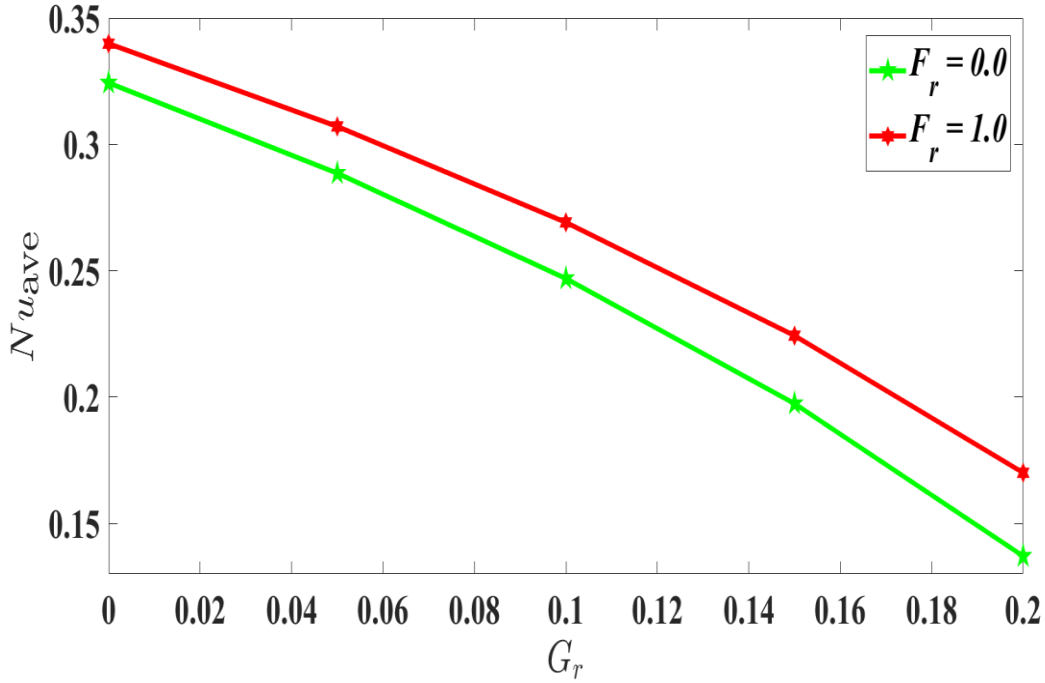

Figure 4. Average Nusselt number profile *versus* buoyancy convection parameter against multiple values of F_r.

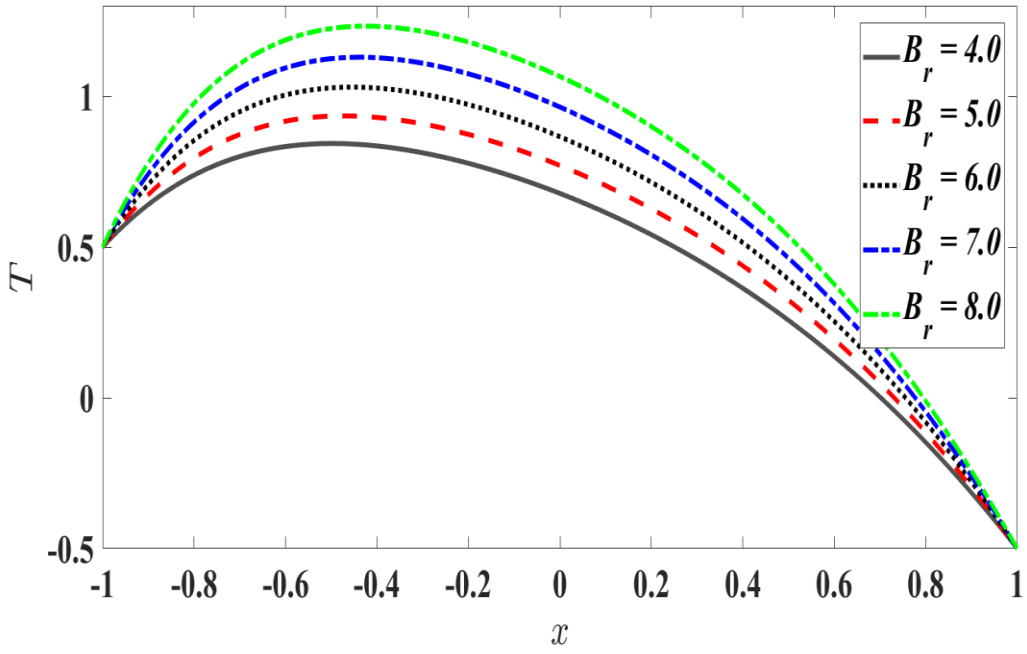

Figure 5. Temperature profile across channel for multiple values of B_r.

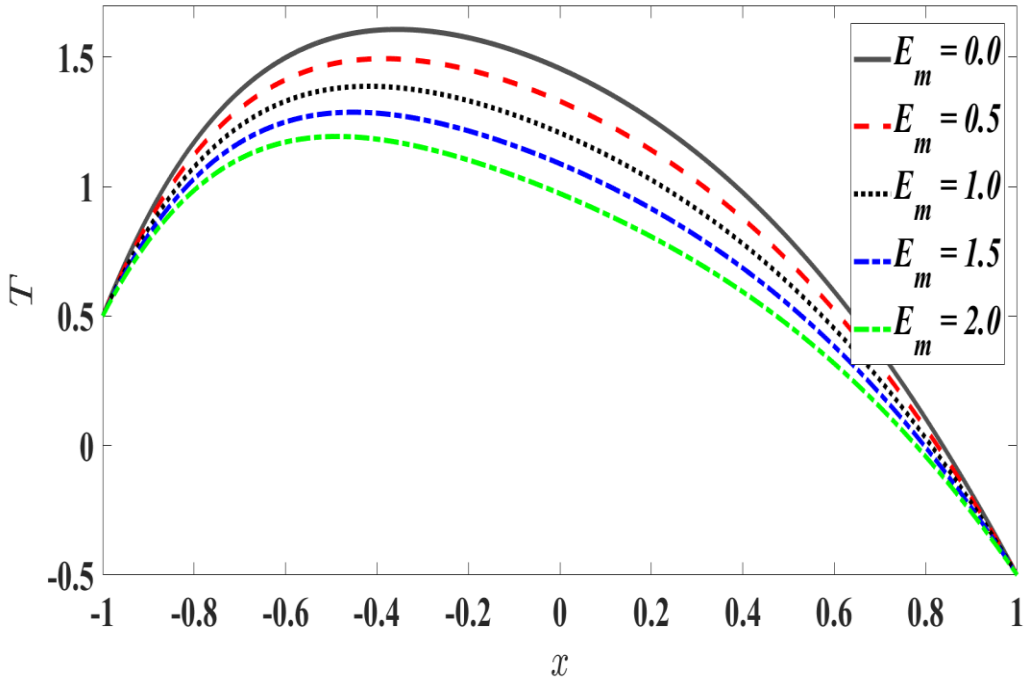

Figure 6. Temperature profile across channel for multiple values of E_m.

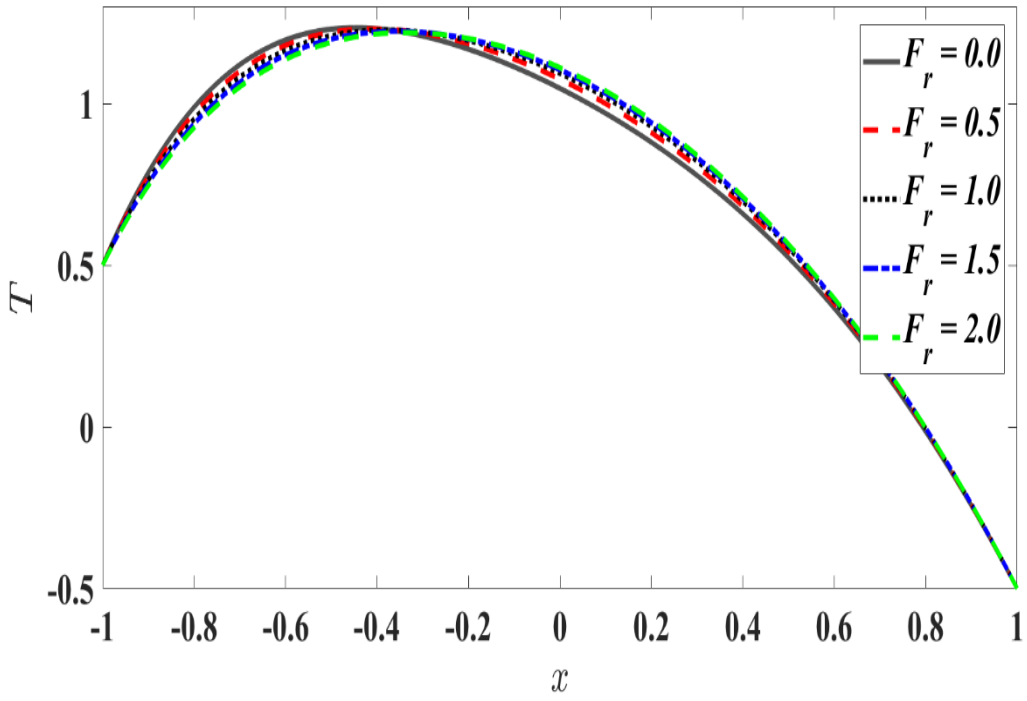

Figure 7. Temperature profile across channel for multiple values of F_r.

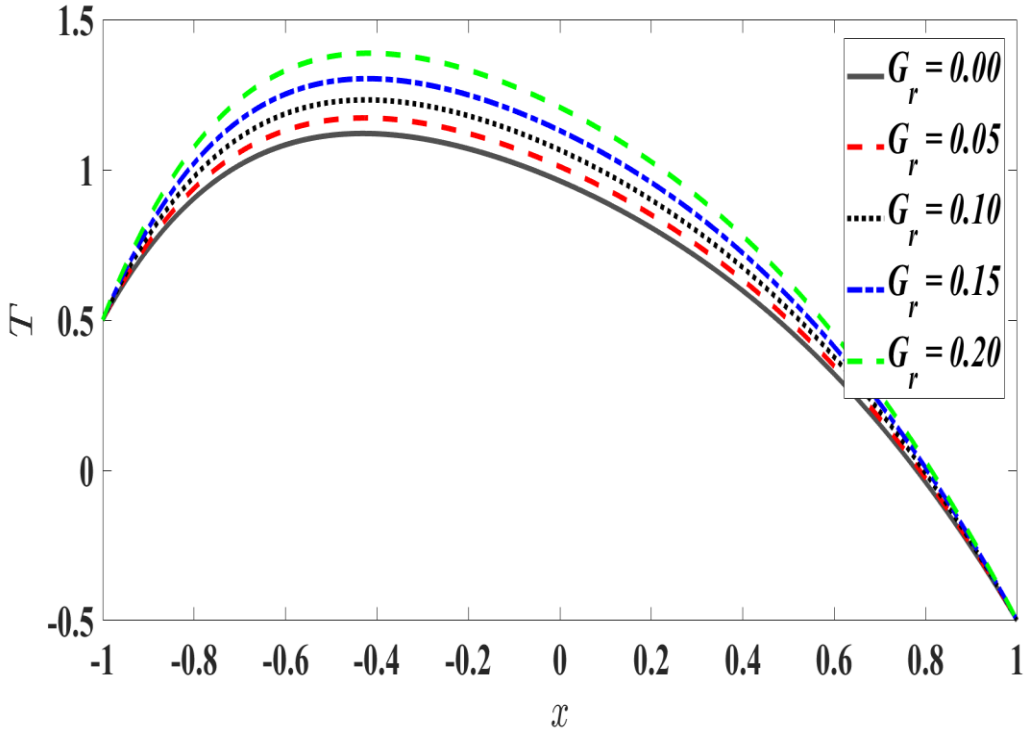

Figure 8. Temperature profile across channel for multiple values of G_r.

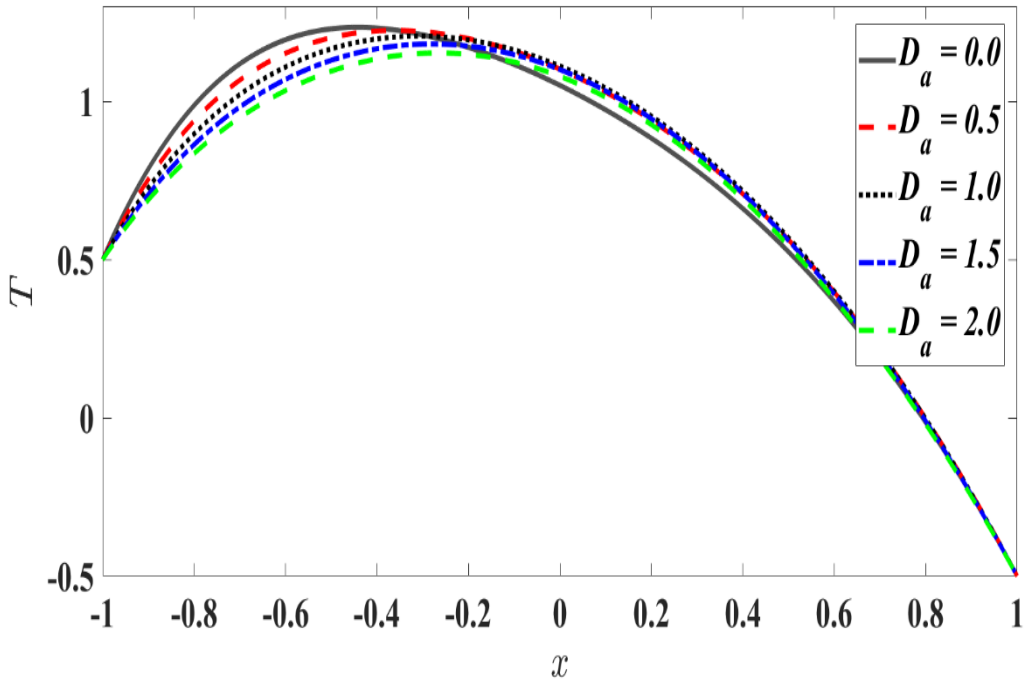

Figure 9. Temperature profile across channel for multiple values of D_a.

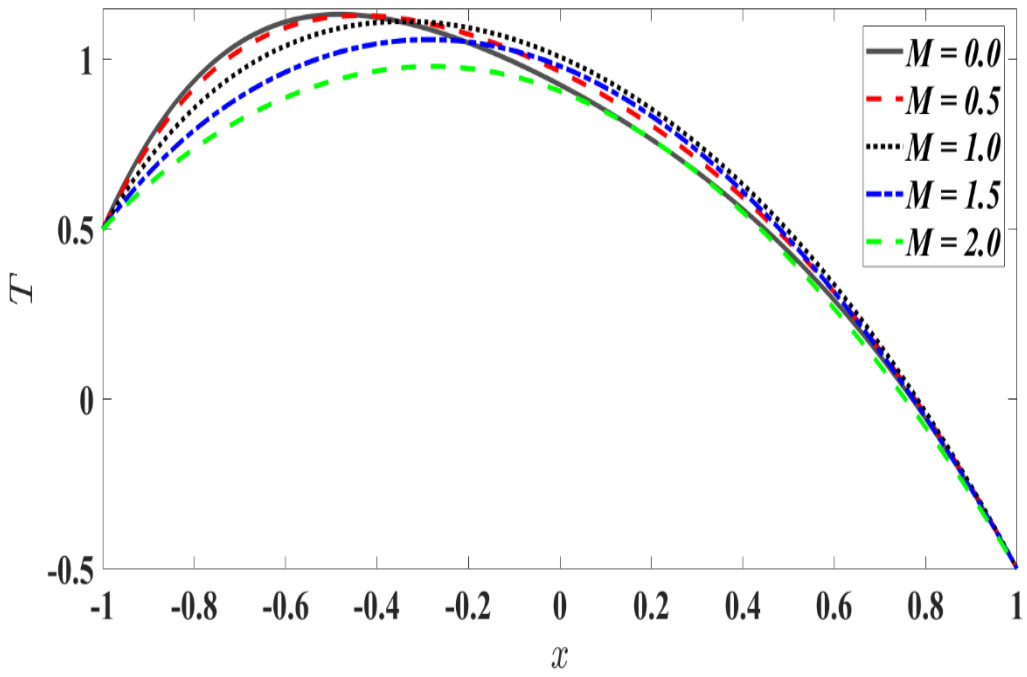

Figure 10. Temperature profile across channel for multiple values of *M*.

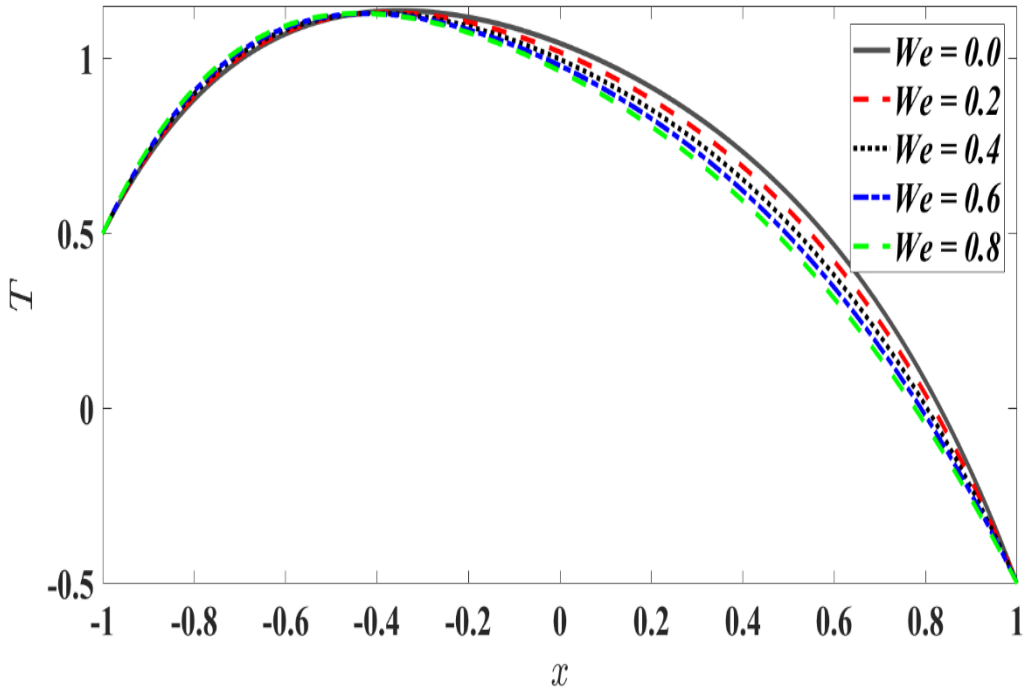

Figure 11. Temperature profile across channel for multiple values of *We*.

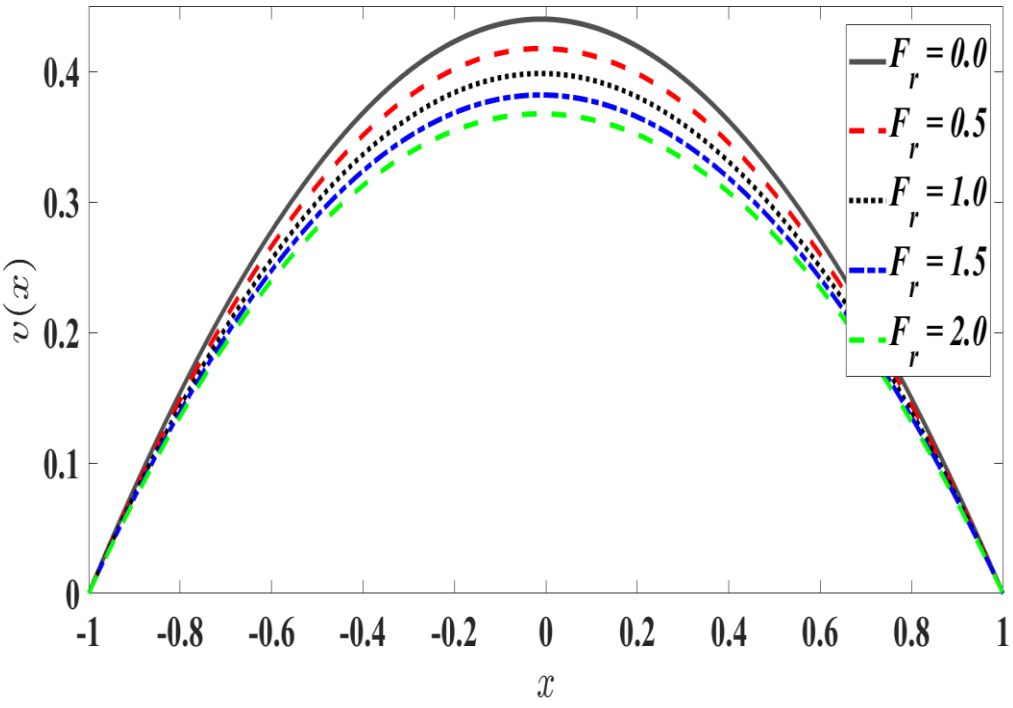

Figure 12. Velocity profile across channel for multiple values of F_r.

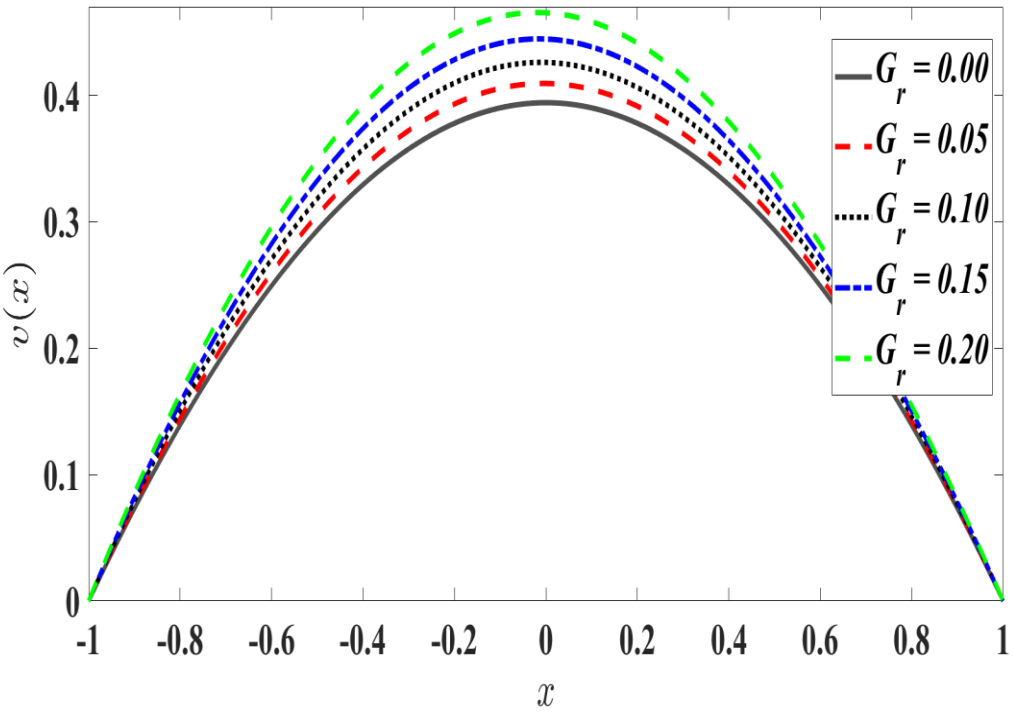

Figure 13. Velocity profile across channel for multiple values of G_r.

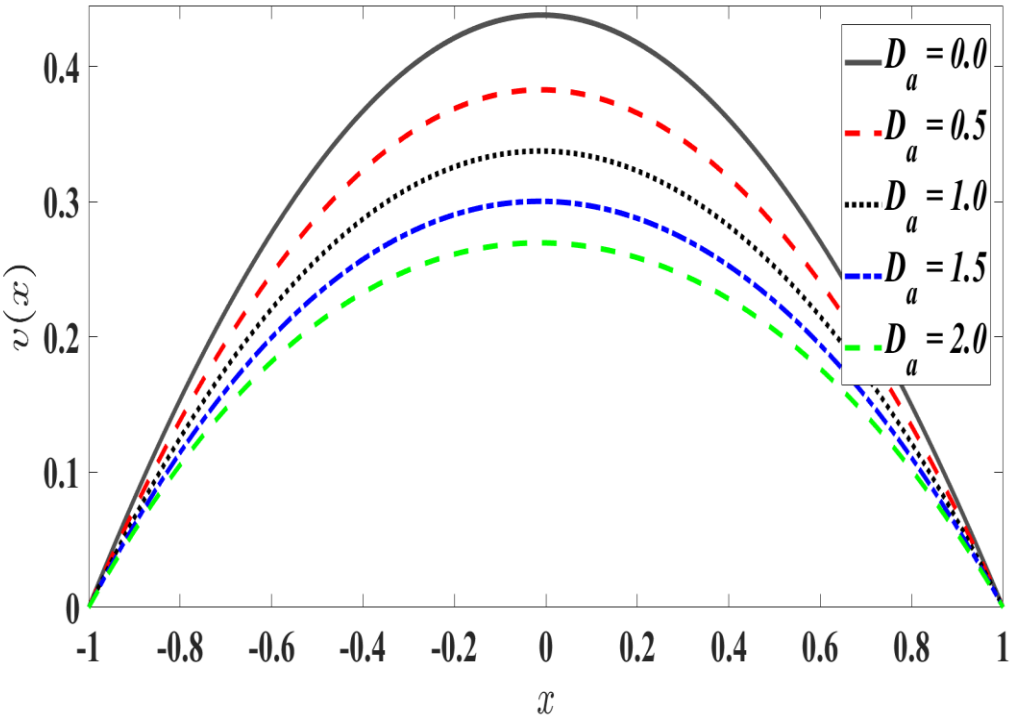

Figure 14. Velocity profile across channel for multiple values of D_a.

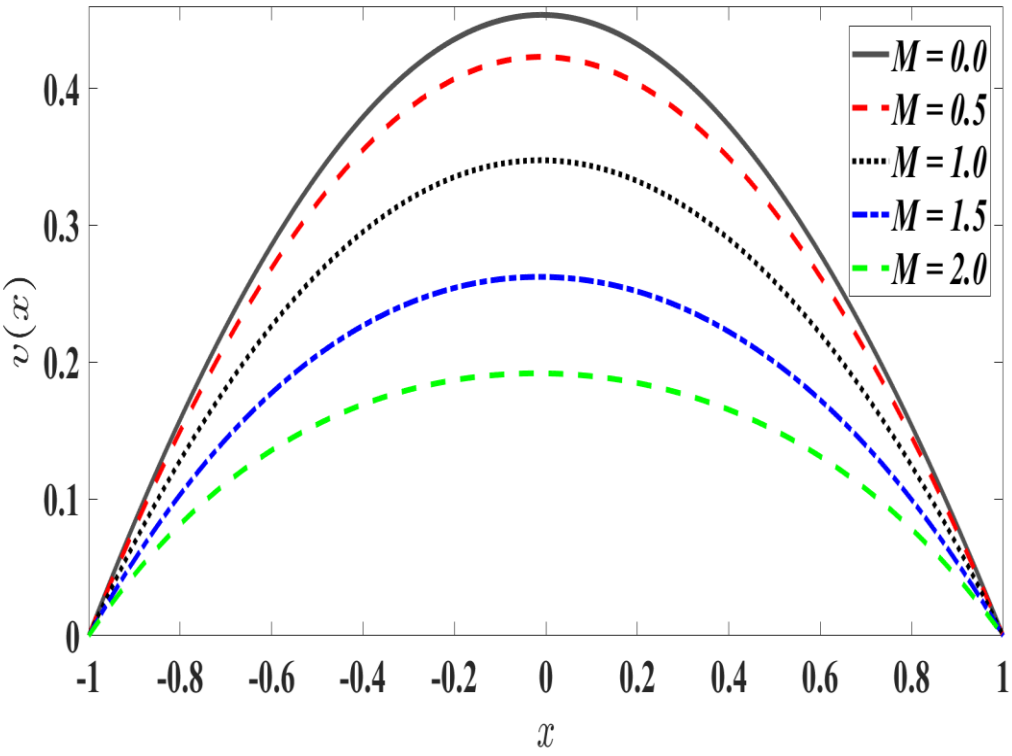

Figure 15. Velocity profile across channel for multiple values of *M*.

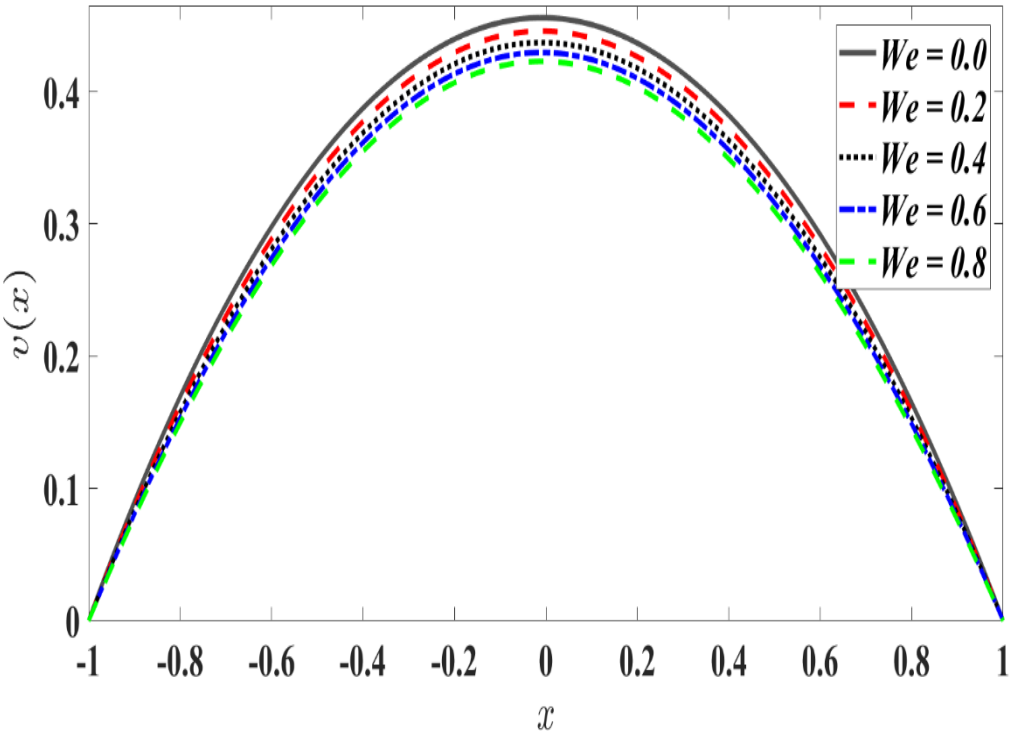

Figure 16. Velocity profile across channel for multiple values of *We*.

The average Nusselt number profile *vs* the Brinkman number B_r for various E_m values is presented in **Figure 2.** As the Brinkman number is growing, the average Nusselt number magnitude steadily decreases; nevertheless, increment in E_m improves the average Nusselt number values. Brinkman number $B_r = \frac{\mu V_0^2}{T_c(\tilde{T}_- - \tilde{T}_+)}$ features in multiple terms in the energy eqn. (12), namely $B_r\left(\frac{dv}{d\bar{x}}\right)\left[\frac{dv}{d\bar{x}} + We\left(\frac{dv}{d\bar{x}}\right)^2\right]$, the electromagnetic Joule heating term, $B_r M^2 v^2$ and the porous medium terms, $D_a B_r v^2 + B_r F_r v^3$. It evidently exerts a significant effect on temperature (and velocity) distributions in realistic polymer flows. Larger Brinkman number (which is also the product of Prandtl number and Eckert number) implies a greater proportion of viscous heat generation relative to external heating. This energizes the electroconductive polymer and enhances temperatures in the bulk fluid. The rate of heat transfer to the duct walls is therefore reduced and manifests in a reduction in Nusselt number. The decay is approximately linear. Clearly neglection of viscous dissipation in simulations of polymer heat transfer leads to an over-prediction in Nusselt numbers. The increment in E_m implies a greater contribution in Joule heating relative to thermal conduction. This encourages heat diffusion to the duct walls and elevates average Nusselt number magnitudes.

The impact of Hartmann magnetic number, M and the Darcy number D_a on average Nusselt number profiles is depicted in **Figure 3**. It is noticed that there is a sustained increment in average Nusselt number with greater M values. Convection heat transfer therefore dominates conduction heat transfer with stronger Lorentz magnetic body force. The intensity of magnetic field growing therefore leads to an intensification in heat transferred to the duct wall. At weak magnetic field levels (low M), the average Nusselt number profile increases first due to an increase in Darcy number. However, when magnetic fields become stronger (e.g., $M > 3.5$), the influence of Darcy number on the average Nusselt number profile becomes much less prominent. Larger Darcy number implies greater permeability of the porous medium and an associated decrease in solid matrix fibers. This stifles thermal conduction but encourages thermal convection leading to greater heat transferred to the walls of the duct and higher Nusselt number. Similar effects have been reported by Shenoy [5]. Inspection of **Figure 4** reveals that greater values of the Grashof number G_r distinctly reduce the average Nusselt number values. Stronger thermal buoyancy relative to viscous hydrodynamic force in the regime therefore inhibits noticeably the transfer of thermal energy to the duct boundaries. This is due to the energizing of the polymer bulk fluid regime which elevates temperatures. Transfer of heat therefore is intensified from the boundaries to the internal regime. With increment in Forchheimer number F_r augments the average number profile. Stronger inertial drag decelerates the bulk flow in the channel via the quadratic resistance generated by the term, $-F_r v^2$, in the momentum eqn. (11). This inhibits both

upward motion of the polymer and induces a cooling effect. Forchheimer number F_r also features in the modified viscous heating term, $+B_r F_r v^3$ in the energy eqn. (12). Effectively greater Forchheimer drag in the porous medium encourages heat transfer to the duct walls and produces greater average Nusselt numbers.

Figures 5-11 illustrate the temperature evolution across the channel (duct) i. e. with x-coordinate and key parameters. As seen in **Figure 5**, the temperature profile increases as the Brinkman number B_r increases. When the Brinkman number is increased, greater kinetic energy is converted to thermal energy via molecular collisions in the electro-conductive polymer flow. Convection is amplified with respect to thermal conduction, and the temperatures are boosted across the channel. The asymmetric parabolic profiles are due to different wall temperature prescribed at the left and right walls. Peak temperature is closer to the left hot wall and is slightly displaced further from it with increasing Brinkman number. In **Figure 6**, we see that the temperature profile has been greatly lowered as a result of the increased influence of E_m. $E_m = \frac{2\sigma EBV_0 b^2}{T_c(\tilde{T}_- - \tilde{T}_+)}$ and as noted before symbolizes the ratio of Joule heating to heat conduction. It features only in the resistive body force term, $-E_m v$, in the energy eqn. (10) which is coupled to the momentum eqn. (11). As this term is increased in magnitude, thermal conduction is suppressed, and the regime is cooled. This is distinct from the classical Hartmann number in which temperatures are elevated with stronger magnetic field. The interaction of electrical and magnetic fields, as in the present simulations, produces a different effect. Asymmetry is again observed in the temperature curves and the peak temperature again migrates towards the right wall of the duct with stronger E_m values. **Figure 7** indicates that with increment in Forchheimer parameter, F_r temperature profile increases significantly when $x > -0.3$, whereas it is weakly reduced when $x < -0.3$. Here, $x = -0.3$ is a critical point in the whole domain. The inertial quadratic drag therefore produces a different behaviour near the left wall compared with the core region of the duct. This may be related to the distribution of solid matrix fibres in the porous medium and furthermore to the packing of material near the boundary where vorticity diffusion (Brinkman friction) is more prominent. As illustrated in **Figure 8**, elevation in the buoyancy convection parameter G_r boosts the temperature profile equally over the whole region. The Grashof number denotes the ratio of buoyancy to viscous forces acting on a working fluid. Physically, it demonstrates that buoyancy forces dominate the viscous forces, and energize the regime via more intensive natural convection currents. For the case of $G_r = 0$, thermal buoyancy vanishes and forced convection is present in the regime. This produces minimal temperatures. Profiles are strongly skewed towards the left duct wall and maximum temperature in this case are shifted closer to this boundary with greater values of buoyancy convection parameter. In **Figure 9**, it is apparent that elevation in the Darcy number D_a strongly reduces temperature magnitudes

when x < -0.2, but in the remaining interval it weakly enhances the temperature profile. Modification in permeability therefore exerts a variable effect across the channel on the temperature distribution. Closer to the left wall, a cooling effect is induced with greater permeability whereas in the core region a heating effect is produced. The asymmetry in temperature profiles is again clearly observed. **Figure 10** demonstrates that with an increase in the Hartmann number M, there is a strong decrement in temperatures across the channel width. Stronger magnetic field therefore generates a cooling effect, which is distinct from classical Hartmann flow where electrical field is absent. Maximum temperature is computed in the left half space, near the left wall for the non-magnetic case (M = 0), although in the right half space this scenario also produces low temperatures. Magnetic field therefore exerts an inconsistent influence across the channel, which is complex due to the interplay with electrical field applied in the axial direction and collective effects of Joule dissipation and thermal buoyancy. This has also been identified in other studies including Yamaguchi *et al.* [46] and Tripathi *et al*. [54]. **Figure 11** shows that with greater values of the Weissenberg number *We*, temperature magnitudes are initially slightly enhanced near the left duct region whereas they are substantially depleted in the core region of the channel and towards the right duct wall. As the Weissenberg number increases, elastic forces become more substantial than viscous forces. $We = \frac{\sqrt{2}V_0\Lambda}{b}$ and features both in the momentum eqn. (10) and in the energy eqn. (11) in the terms, $+We\frac{d^2v}{dx^2}\left(\frac{dv}{dx}\right)$ and $B_r\left(\frac{dv}{d\bar{x}}\right)\left[We\left(\frac{dv}{d\bar{x}}\right)^2\right]$, respectively. This produces a complex response in which boundary layer development at the duct walls is strongly influenced. There is therefore a delay in the transfer of heat with greater elastic forces as one progresses across the channel, which explains the initial slight increase in temperatures which is eventually dominated by a strong reduction in temperatures further into the duct towards the core zone. Stress relaxation is also described by the Weissenberg number. It may also be considered as the ratio of stress relaxation time to the process time, under shearing. The black line in this Figure depicts the *Newtonian fluid* obtained by assuming We = 0 in Eqs (11-12). This special case achieves the maximum temperatures for the majority of the span of the channel. Clearly when non-Newtonian effects are neglected, temperatures are over-predicted. The deployment of a good rheological model i. e. Williamson model, as in the current study, achieves more realistic computations for polymer thermofluid mechanical simulations. In turn, these provide engineers with better approximations of the actual thermal transport in electro-conductive rheological duct flows.

Figures 12-16 depict the evolution in fluid velocity across the channel width as a function of several key parameters. **Figure 12** shows that when the Forchheimer parameter F_r grows, the velocity profile decreases dramatically. The quadratic drag is amplified with an increase in this parameter as inertial effects dominate viscous effects. Stronger damping

forces are generated to the percolation of the polymeric fluid in the porous medium as a result of higher F_r values, generating significant deceleration in the flow. This effect is sutained across the channel. The classical Darcian case is retrieved for $Fr = 0$ and clearly achieves the maximum velocity. Neglection of Forchheimer effect therefore leads to a marked over-prediction in velocity in the duct. **Figure 13** indicates the impact of the buoyancy convection parameter G_r on the velocity profile. It can be observed that an accentuation in thermal buoyancy force therefore substantially accelerates the flow across the channel width. Natural convection currents are intensified with thermal buoyancy forces which aids in momentum development in the regime. **Figure 14** shows that increment in Darcy number D_a considerably restricts fluid flow over the whole channel, while the highest fluid velocity is recorded at the center of the parallel plates. Increasing permeability therefore produces a very different effect with the non-Darcy formulation used here, compared with conventional models in which greater permeability will produce flow acceleration. The presence of Darcy number in other terms e.g. $+D_a B_r v^2$ in eqn. (11) contributes to the overall retardation induced in the flow. **Figure 15** depicts the effect of the Hartmann (magnetic) parameter, M on the velocity profile. It can be seen here that the magnetic field has a considerable effect on the fluid velocity. The presence of a stronger magnetic field damps the velocity i.e. induces deceleration. This effect is sustained across the channel. aids in the control of fluid movements. With greater M values the Lorentz magnetic drag dominates the viscous force in the regime. For the case $M = 1$ both forces contribute equally. Maximum velocity is achieved in the absence of transverse magnetic field ($M = 0$). **Figure 16** depicts the influence of the Weissenberg number We on velocity profile. When $We = 0$, this case corresponds to Newtonian behavior. We can observe that when the Weissenberg number grows, the velocity profile drops, indicating that elastic forces exceed the viscous forces. The polymer therefore flows with reduced resistance in the duct and experiences strong acceleration.

7. CONCLUSIONS

A mathematical model has been developed for natural convection electro-magneto-hydrodynamic non-Newtonian Williamson flow between vertical parallel plates containing a permeable medium. The effects of viscous dissipation and natural convection have been included in the energy equation. The momentum equation features a modified Darcy-Brinkman-Forchheimer model in which viscous dissipation terms are refined for the effect of viscous heating. Mutually orthogonal electrical and magnetic fields are considered. Joule heating is also addressed. The conservation equations with associated boundary conditions are re-framed into a system of coupled non-linear ordinary differential equations via appropriate similarity transformations. The emerging dimensionless boundary value problem

is then solved with a differential transform method (DTM). Validation of DTM solutions with the bvp4c MATLAB collocation solver is included. The influence of key parameters on velocity, temperature and average Nusselt number, are computed and illustrated graphically. The key findings of the present simulation may be summarized as follows:

(i)With elevation in Weissenberg (non-Newtonian) number, velocity is significantly suppressed across the channel.

(ii)Velocity is suppressed with increasing non-Darcian parameter (Forchheimer number) whereas it is enhanced with increment in buoyancy convection parameter.

(iii)With increasing Forchheimer, Darcy number and Hartmann (magnetic) number, the *average Nusselt number* is boosted whereas it is decreased with higher values of buoyancy convection parameter, Brinkman number, and Weissenberg number.

(iv) A strong reduction in temperature is computed with increment in ratio of Joule electrical heating to heat conduction parameter.

(v) With increasing Forchheimer (non-Darcian) and Darcy number, there is a strong reduction in temperatures near the duct left wall but a significant elevation in the core region of the duct.

(vi)With greater Weissenberg number, temperatures are initially increased near the left wall of the duct and then substantially reduced in the core region and towards the right wall of the duct.

(vii)Temperatures are significantly enhanced across the duct width with increment in Brinkman number (viscous heating parameter).

(viii) The inclusion of a modified non-Darcy model and robust Williamson viscoelastic model is shown to more accurately capture the characteristics of electroconductive polymer duct heat transfer flows.

(ix) DTM is demonstrated to be an exceptionally accurate and versatile methodology for solving nonlinear boundary value problems appropriate to non-Newtonian electromagnetohydrodynamic transport in ducts.

The present study has neglected mass (species) diffusion effects. These may be considered in future investigations using both Fickian and non-Fickian models.

FUNDING: Lijun Zhang and M. M. Bhatti are supported by the National Natural Science Foundation of China No. 12172199.

REFERENCES

[1] Y. Jaluria, *Natural Convection: Heat and Mass Transfer***,** 326pp, Elsevier Science & Technology, USA (1980).

[2] Yovanovich, M. M., Teertstra, P., & Muzychka, Y. S. (2002). Natural convection inside vertical isothermal ducts of constant arbitrary cross section. *Journal of thermophysics and heat transfer*, *16*(1), 116-121.
[3] Gonzalez-Hidalgo, C. T., Herrero, J., & Puigjaner, D. (2012). Mixing intensification by natural convection with application to a chemical reactor design. *Chemical engineering journal*, *200*, 506-520.
[4] Chhabra, R.; Richardson, J. *Non-Newtonian Flow and Applied Rheology*: Engineering Applications, 2nd ed.; Butterworth-Heinemann: Oxford, UK (2008).
[5] Shenoy, A. V. (1994). Non-Newtonian fluid heat transfer in porous media. In *Advances in Heat transfer*, 24, 101-190.
[6] Haghighi, S. S., Goshayeshi, H. R., & Safaei, M. R. (2018). Natural convection heat transfer enhancement in new designs of plate-fin based heat sinks. *International Journal of Heat and Mass Transfer*, *125*, 640-647.
[7] Dutta, S., Biswas, A. K., & Pati, S. (2018). Natural convection heat transfer and entropy generation inside porous quadrantal enclosure with non-isothermal heating at the bottom wall. *Numerical Heat Transfer, Part A: Applications*, *73*(4), 222-240.
[8] Ma, Y., Mohebbi, R., Rashidi, M. M., & Yang, Z. (2019). Effect of hot obstacle position on natural convection heat transfer of MWCNTs-water nanofluid in U-shaped enclosure using lattice Boltzmann method. *International Journal of Numerical Methods for Heat & Fluid Flow*. *29*(1), 223-250.
[9] Nia, S. N., Rabiei, F., Rashidi, M. M., & Kwang, T. M. (2020). Lattice Boltzmann simulation of natural convection heat transfer of a nanofluid in a L-shape enclosure with a baffle. *Results in Physics*, *19*, 103413.
[10] Jha, B. K., & Samaila, G. (2020). A similarity solution for natural convection flow near a vertical plate with thermal radiation. *Microgravity Science and Technology*, *32*(6), 1031-1038.
[11] Dash, M. K., & Dash, S. K. (2020). Natural convection heat transfer and fluid flow around a thick hollow vertical cylinder suspended in air: a numerical approach. *International Journal of Thermal Sciences*, *152*, 106312.
[12] Dutta, S., Goswami, N., Pati, S., & Biswas, A. K. (2021). Natural convection heat transfer and entropy generation in a porous rhombic enclosure: influence of non-uniform heating. *Journal of Thermal Analysis and Calorimetry*, *144*(4), 1493-1515.
[13] Lee, S. R., Irvine Jr, T. F., & Greene, G. A. (1998). A Computational Analysis of Natural Convection in a Vertical Channel with a Modified Power Law Non-Newtonian Fluid. In *International Heat Transfer Conference Digital Library*. Begel House Inc.
[14] Jangili, S., & Bég, O. A. (2018). Homotopy study of entropy generation in magnetized micropolar flow in a vertical parallel plate channel with buoyancy effect. *Heat Transfer Research*, *49*(6), 529-553.
[15] Singh, J. K., Seth, G. S., Joshi, N., & Srinivasa, C. T. (2020). Mixed convection flow of a viscoelastic fluid through a vertical porous channel influenced by a moving magnetic field with Hall and ion-slip currents, rotation, heat radiation and chemical reaction. *Bulgarian Chemical Communications*, *52*(1), 147-158.

[16] Bég, O. A., Takhar, H. S., Bég, T. A., Bhargava, R., & Rawat, S. (2008). Nonlinear magneto-heat transfer in a fluid-particle suspension flowing in a non-Darcian channel with heat source and buoyancy effects: numerical study. *Engineering Sciences*, *19*(1).

[17] Yang, W. J., & Yeh, H. C. (1965). Free convective flow of Bingham plastic between two vertical plates, *Trans. ASME, Journal of Heat Transfer*, 87, 319.

[18] Rajagopal, K. R., & Na, T. Y. (1985). Natural convection flow of a non-Newtonian fluid between two vertical flat plates. *Acta Mechanica*, *54*(3), 239-246.

[19] Manzoor, N., Bég, O. A., Maqbool, K., & Shaheen, S. (2019). Mathematical modelling of ciliary propulsion of an electrically-conducting Johnson-Segalman physiological fluid in a channel with slip. *Computer methods in biomechanics and biomedical engineering*, *22*(7), 685-695.

[20] Gebhart, B. (1962). Effects of viscous dissipation in natural convection. *Journal of fluid Mechanics*, *14*(2), 225-232.

[21] Martin, B. W. (1973). Viscous heating and varying viscosity effects on developing laminar flow in a circular pipe. *Proceedings of the Institution of Mechanical Engineers*, *187*(1), 435-445.

[22] Salah El-Din, M. M. (2002). Effect of viscous dissipation on laminar mixed convection in a horizontal channel. *Proceedings of the Institution of Mechanical Engineers, Part E: Journal of Process Mechanical Engineering*, *216*(3), 167-172.

[23] Umavathi, J. C., & Anwar Bég, O. (2020). Mathematical Modelling of Triple Diffusion in Natural Convection Flow in a Vertical Duct with Robin Boundary Conditions, Viscous Heating, and Chemical Reaction Effects. *Journal of Engineering Thermophysics*, *29*(2), 348-373.

[24] Shamshuddin, M. D., Mishra, S. R., Bég, O. A., & Kadir, A. (2019). Viscous dissipation and joule heating effects in non-Fourier MHD squeezing flow, heat and mass transfer between Riga plates with thermal radiation: variational parameter method solutions. *Arabian Journal for Science and Engineering*, *44*(9), 8053-8066.

[25] Ajibade, A. O., & Umar, A. M. (2020). Effects of viscous dissipation and boundary wall thickness on steady natural convection Couette flow with variable viscosity and thermal conductivity. *International Journal of Thermofluids*, *7*, 100052.

[26] Cox, H. W., & Macosko, C. W. (1974). Viscous dissipation in die flows. *AIChE Journal*, *20*(4), 785-795.

[27] Winter, H. H. (1977). Viscous dissipation in shear flows of molten polymers. In *Advances in Heat Transfer* (Vol. 13, pp. 205-267). Elsevier.

[28] Hassan, H., Regnier, N., Pujos, C., & Defaye, G. (2008). Effect of viscous dissipation on the temperature of the polymer during injection molding filling. *Polymer Engineering & Science*, *48*(6), 1199-1206.

[29] Akbar, N. S., Tripathi, D., Bég, O. A., & Khan, Z. H. (2016). MHD dissipative flow and heat transfer of Casson fluids due to metachronal wave propulsion of beating cilia with thermal and velocity slip effects under an oblique magnetic field. *Acta Astronautica*, *128*, 1-12.

[30] Ragueb, H., & Mansouri, K. (2013). A numerical study of viscous dissipation effect on non-Newtonian fluid flow inside elliptical duct. *Energy Conversion and Management*, *68*, 124-132.

[31] Umavathi, J. C., & Bég, O. A. (2021). Augmentation of heat transfer via nanofluids in duct flows using Fourier-type conditions: Theoretical and numerical study. *Proceedings of the Institution of Mechanical Engineers, Part E: Journal of Process Mechanical Engineering*, 09544089211052025.

[32] Nakayama, A., Kokudai, T., & Koyama, H. (1990). Non-Darcian boundary layer flow and forced convective heat transfer over a flat plate in a fluid-saturated porous medium. *ASME Journal of Heat Transfer. 112*, 157–162.

[33] Bear, J., & Braester, C. (1972). On the flow of two immiscible fluids in fractured porous media. In *Developments in Soil Science* (Vol. 2, pp. 177-202). Elsevier.

[34] Nield, D. A., & Bejan, A. (2006). *Convection in Porous Media* (Vol. 3). New York: springer.

[35] L. Royon and G. Guiffant, Forced convection heat transfer with slurry of phase change material in circular ducts: A phenomenological approach, *Energy Conversion and Management*, 49, 928-932 (2008).

[36] Nazari, S., Ellahi, R., Sarafraz, M. M., Safaei, M. R., Asgari, A., & Akbari, O. A. (2020). Numerical study on mixed convection of a non-Newtonian nanofluid with porous media in a two lid-driven square cavity. *Journal of Thermal Analysis and Calorimetry*, *140*(3), 1121-1145.

[37] Muskat, M. (1946). *The Flow of Homogeneous Fluids through Porous Media*. JW Edwards. Ann Arbor, Mich, USA.

[38] Brinkman, H. C. (1949). On the permeability of media consisting of closely packed porous particles. *Flow, Turbulence and Combustion*, *1*(1), 81-86.

[39] Zhao, J., Zheng, L., Zhang, X., Liu, F., & Chen, X. (2017). Unsteady natural convection heat transfer past a vertical flat plate embedded in a porous medium saturated with fractional Oldroyd-B fluid. *Journal of Heat Transfer*, *139*(1).

[40] Tripathi, D., & Bég, O. A. (2012). A numerical study of oscillating peristaltic flow of generalized Maxwell viscoelastic fluids through a porous medium. *Transport in porous media*, *95*(2), 337-348.

[41] Alomar, O. R., Basher, N. M., & Yousif, A. A. (2020). Analysis of effects of thermal non-equilibrium and non-Darcy flow on natural convection in a square porous enclosure provided with a heated L shape plate. *International Journal of Mechanical Sciences*, 181, 105704.

[42] Bég, O. A., Takhar, H. S., Zueco, J., Sajid, A., & Bhargava, R. (2008). Transient Couette flow in a rotating non-Darcian porous medium parallel plate configuration: network simulation method solutions. *Acta Mechanica*, *200*(3), 129-144.

[43] Bég, T. A., Rashidi, M. M., Bég, O. A., & Rahimzadeh, N. (2013). Differential transform semi-numerical analysis of biofluid-particle suspension flow and heat transfer in non-Darcian porous media. *Computer methods in biomechanics and biomedical engineering*, *16*(8), 896-907.

[44] Al-Hadhrami, A.K., Elliott, L., Ingham, D.B.: A new model for viscous dissipation in porous media across a range of permeability values. *Transp. Porous Media* 53, 117–122 (2003).

[45] Umavathi, J. C. (2013). Analysis of flow and heat transfer in a vertical rectangular duct using a non-Darcy model. *Transport in porous media*, *96*(3), 527-545.

[46] Yamaguchi, H., Zhang, X. R., Higashi, S., & Li, M. (2008). Study on power generation using electro-conductive polymer and its mixture with magnetic fluid. *Journal of Magnetism and Magnetic Materials*, *320*(7), 1406-1411.

[47] Castro-Gutiérrez, J., Palaimiene, E., Macutkevic, J., Banys, J., Kuzhir, P., Schaefer, S., Fierro, V. and Celzard, A., (2019). Electromagnetic properties of carbon gels. *Materials*, *12*(24), p.4143.

[48] Shliomis, M., Krekhov, A., & Kamiyama, S. (2006, May). Non-Newtonian Ferrofluid Flow in Oscillating Magnetic Field. In *AIP Conference Proceedings* (Vol. 832, No. 1, pp. 403-411). American Institute of Physics.

[48] Xu, Y., Patsis, P.A., Hauser, S., Voigt, D., Rothe, R., Günther, M., Cui, M., Yang, X., Wieduwild, R., Eckert, K. and Neinhuis, C., (2019). Cytocompatible, injectable, and electroconductive soft adhesives with hybrid covalent/noncovalent dynamic network. *Advanced Science*, *6*(15), p.1802077.

[49] Bhatti, M. M. (2021). Biologically inspired intra-uterine nanofluid flow under the suspension of magnetized gold (Au) nanoparticles: applications in nanomedicine. *Inventions*, *6*(2), 28.

[50] Manzoor, N., Maqbool, K., Bég, O. A., & Shaheen, S. (2019). Adomian decomposition solution for propulsion of dissipative magnetic Jeffrey biofluid in a ciliated channel containing a porous medium with forced convection heat transfer. *Heat Transfer—Asian Research*, *48*(2), 556-581.

[51] Tripathi, D., Yadav, A., & Bég, O. A. (2017). Electro-kinetically driven peristaltic transport of viscoelastic physiological fluids through a finite length capillary: mathematical modeling. *Mathematical Biosciences*, *283*, 155-168.

[52] Bhatti, M. M., Zeeshan, A., Ijaz, N., Bég, O. A., & Kadir, A. (2017). Mathematical modelling of nonlinear thermal radiation effects on EMHD peristaltic pumping of

viscoelastic dusty fluid through a porous medium duct. *Engineering science and technology, an international journal*, *20*(3), 1129-1139.

[53] Umavathi, J. C., & Bég, O. A. (2021). Double-diffusive convection in a dissipative electrically conducting nanofluid under orthogonal electric and magnetic fields: a numerical study. *Nanoscience and Technology: An International Journal*, *12*(2), 59-90.

[54] Tripathi, D., Jhorar, R., Bég, O. A., & Kadir, A. (2017). Electro-magneto-hydrodynamic peristaltic pumping of couple stress biofluids through a complex wavy micro-channel. *Journal of Molecular Liquids*, *236*, 358-367.

[55] Tripathi, D., Bhushan, S., & Bég, O. A. (2016). Transverse magnetic field driven modification in unsteady peristaltic transport with electrical double layer effects. *Colloids and Surfaces A: Physicochemical and Engineering Aspects*, *506*, 32-39.

[56] Vajravelu, K., Sreenadh, S., Rajanikanth, K., & Lee, C. (2012). Peristaltic transport of a Williamson fluid in asymmetric channels with permeable walls. *Nonlinear Analysis: Real World Applications*, *13*(6), 2804-2822.

[57] Amanulla, C. H., Nagendra, N., Subba Rao, A., Anwar Bég, O., & Kadir, A. (2018). Numerical exploration of thermal radiation and Biot number effects on the flow of a non-Newtonian MHD Williamson fluid over a vertical convective surface. *Heat Transfer—Asian Research*, *47*(2), 286-304.

[58] Subba Rao, A., Amanulla, C. H., Nagendra, N., Anwar Beg, O., & Kadir, A. (2017). Hydromagnetic flow and heat transfer in a Williamson Non-Newtonian fluid from a Horizontal circular cylinder with Newtonian Heating. *International Journal of Applied and Computational Mathematics*, *3*(4), 3389-3409.

[59] Zhou, J. K. (1986). *Differential Transformation and its Applications for Electrical Circuits*. Huazhong Science & Technology University Press, China.

[60] Faraz, N., Khan, Y., Lu, D. C., & Goodarzi, M. (2019). Integral transform method to solve the problem of porous slider without velocity slip. *Symmetry*, *11*(6), 791.

[61] Maleki, H., Alsarraf, J., Moghanizadeh, A., Hajabdollahi, H., & Safaei, M. R. (2019). Heat transfer and nanofluid flow over a porous plate with radiation and slip boundary conditions. *Journal of Central South University*, *26*(5), 1099-1115.

[62] Maleki, H., Safaei, M. R., Alrashed, A. A., & Kasaeian, A. (2019). Flow and heat transfer in non-Newtonian nanofluids over porous surfaces. *Journal of Thermal Analysis and Calorimetry*, *135*(3), 1655-1666.

[63] Zhang, L., Arain, M. B., Bhatti, M. M., Zeeshan, A., & Hal-Sulami, H. (2020). Effects of magnetic Reynolds number on swimming of gyrotactic microorganisms between rotating circular plates filled with nanofluids. *Applied Mathematics and Mechanics*, 41(4), 637-654.

[64] Arain, M. B., Bhatti, M. M., Zeeshan, A., & Alzahrani, F. S. (2021). Bioconvection Reiner-Rivlin nanofluid flow between rotating circular plates with induced magnetic effects, activation energy and squeezing phenomena. *Mathematics*, *9*(17), 2139.

[65] Kumar, M., Reddy, G. J., Kumar, N. N., & Bég, O. A. (2019). Application of differential transform method to unsteady free convective heat transfer of a couple stress fluid over a stretching sheet. *Heat Transfer—Asian Research*, *48*(2), 582-600.

[66] Pourhoseini, S. H. (2017). A comparative exploration of enhancing thermal characteristics of natural gas flame by synchronous combustion technique. *Heat Transfer—Asian Research*, *46*(3), 237-250.

[67] Dey, D., & Chutia, B. (2022). Two-phase fluid motion through porous medium with volume fraction: An application of MATLAB bvp4c solver technique. *Heat Transfer*, *51*(2), 1778-1789.

[68] Humane, P. P., Patil, V. S., Patil, A. B., Shamshuddin, M. D., & Rajput, G. R. (2022). Dynamics of multiple slip boundaries effect on MHD Casson-Williamson double-diffusive nanofluid flow past an inclined magnetic stretching sheet. *Proceedings of the Institution of Mechanical Engineers, Part E: Journal of Process Mechanical Engineering*, 09544089221078153.